Actuator Allocation with Adaptive Estimation of Time-Varying Uncertain Parameters for Nonlinear Burn Control

Vincent Graber and Eugenio Schuster

Abstract— **The ITER tokamak will produce energy through the nuclear fusion that can occur when an ionized gas, or plasma, is brought to extreme temperatures. To drive the plasma to regimes that allow net-positive power output, burn control algorithms regulate the plasma's temperature and density by requesting external heating and fueling. These control requests can be satisfied with various actuators. In this work, a model-based, nonlinear burn control algorithm is synthesized along with an optimal actuator allocation algorithm that manages ITER's actuators. This actuator allocation algorithm considers actuator delays and various other complex phenomena, such as the fueling contribution from neutral beam injection (NBI), when searching for the optimal mapping between the burn control algorithm's requests and the available actuators. The burn control and actuator allocation algorithms are based on control-oriented models for the plasma and actuators that include uncertainty. Uncertainty is modeled by asserting that the value of specific parameters are not known to the algorithms. In the model of the plasma system, these uncertain parameters describe the quality of the plasma confinement and plasma-wall effects such as impurity sputtering. In the models for the actuator systems, there are state-dependent, time-varying uncertainties such as the NBI thermalization delay, the uneven NBI power deposition between ions and electrons, and the pellet fueling efficiency. Both the burn control and actuator allocation algorithms are designed to handle these uncertain parameters through adaptive estimation. A simulation study illustrates the capability of these algorithms working together.**

I. INTRODUCTION

The ITER tokamak will magnetically confine burning plasmas, which are very hot ionized gases where deuterium (D) and tritium (T) fuse to create alpha particles and neutrons [1]. The actuators that will be available to ITER include the ion cyclotron (IC) system, the electron cyclotron (EC) system, two neutral beam injectors (NBI), two pellet injectors, and the gas fueling system [2]. Because ITER's NBI actuators heat the plasma by firing highly energetic D particles into it [3], they will contribute to the plasma fueling. While the NBI particles are thermalizing, their energy will be unevenly divided between the plasma's ions and electrons [1]. One of the pellet injectors will fire 100% D pellets, while the other will fire pellets with an approximately 10%D$-$90%T mixed composition [4]. Gas injection will also provide fueling but with less efficiency and longer delays than pellets [4], [5].

Nonlinear burn control algorithms [6], [7] determine the amounts of external heating and fueling required to bring a plasma to a desirable regime in temperature-density space [8], [9]. Burn control is made more challenging due to the nonlinear, coupled dynamics of the plasma system. For example, the positive correlation between the ion temperature and the fusion reaction rate can cause destabilizing feedback loops. The control requests for heating and fueling can be met using the aforementioned suite of ITER actuators. Proficient management of these actuators [10] is critical for meeting control objectives. In [11], a management system was devised to prioritize (possibly competing) control tasks, allocate actuator resources to various controllers, and handle disruptive plasma events. The management system in [12] addresses specific actuator intricacies such as neutral beam shine through which can potentially damage the first wall.

In prior work [13], [14], Lyapunov techniques [15] were used to synthesize burn control algorithms from a nonlinear plasma model. Furthermore, actuator allocation algorithms were designed to optimally map the control requests to ITER's actuators. This mapping between the control requests and actuators is called the effector system [16]. Optimal allocation [17], [18] can assure that the control requests are satisfied when adequate external heating and fueling is available. The actuator allocation algorithm in [14] was designed to deal with actuator dynamics in the form of actuation lag. The models for the plasma, effector and actuator systems included parameters that were considered to be uncertain. A parameter is uncertain if its value is unknown to the algorithms. These uncertain parameters included constants that characterized the DT wall recycling, the actuator efficiencies, the actuator lags, and the T concentration in the fueling pellets.

This work improves upon the actuator allocation algorithm from the prior work [14] in various ways. Firstly, the effector system model now considers the D fueling contribution from NBI. Secondly, the gas fueling system is now included as an actuator. Thirdly, the following parameters in the models for the effector and actuator systems that were considered to be constant in the prior work [14] are now time-varying and state-dependent: the pellet fueling efficiencies, the fractions of the NBI power deposited into the ion and electron populations, and the thermalization delay of the NBI particles.

The paper is organized as follows. The closed-loop system is described in Section II. The model of the plasma system is given in Section III. In Section IV, burn control objectives are drawn. The burn control algorithm is designed in Section V. In Section VI, the model of the effector system is given. The models for the actuator systems are shown in Section VII. The actuator allocation algorithm is provided in Section VIII. In Section IX, low-level actuator control algorithms are designed. A simulation study is presented in Section X. Conclusions and future work are stated in Section XI.

This work was supported in part by the U.S. Department of Energy (DE-SC0010661). V. Graber (graber@lehigh.edu) and E. Schuster are with the Department of Mechanical Engineering and Mechanics, Lehigh University, Bethlehem, PA 18015, USA.

II. THE CLOSED-LOOP SYSTEM

The closed-loop system in Fig. 1 is described as follows. Using the plasma system's states x, the nonlinear burn control algorithm (Section V) calculates the requested stabilizing control efforts v_r that will drive the plasma to a targeted regime. The vector v_r contains requests for ion heating ($P^{req}_{aux,i}$), electron heating ($P^{req}_{aux,e}$), D fueling (S^{req}_D), and T fueling (S^{req}_T). The optimal actuator allocation algorithm (Section VIII) receives v_r and maps it to ITER's actuators. The powers and fueling rates produced by the actuators are termed actuator efforts. The output of the actuator allocation algorithm, the desired actuator efforts u_d, should closely reproduce v_r. In the vector u_d, the desired powers and fueling rates from the IC, EC, NBI, D pellet, DT pellet, and DT gas systems are denoted as P^{des}_{ic}, P^{des}_{ec}, $P^{des}_{nbi_1}$ and $P^{des}_{nbi_2}$, $S^{des}_{D_{pel}}$, $S^{des}_{DT_{pel}}$, and $S^{des}_{DT_{gas}}$, respectively. With the aim of tracking u_d, low-level actuator control algorithms (Section IX) compute the command vector u_{cmd} (which contains P^{cmd}_{ic}, P^{cmd}_{ec}, etc.). Based on their commands u_{cmd}, the actuator systems (Section VII) output their delayed actuator efforts u (P_{ic}, P_{ec}, etc.). Through the effector model (Section VI), u is converted into the control efforts v ($P_{aux,i}$, $P_{aux,e}$, etc.) that evolve the plasma system. Adaptive estimation is used to deal with the uncertain parameters in the models for the plasma, effector, and actuator systems (θ_h, θ_e, and θ_u).

III. THE NONLINEAR PLASMA SYSTEM

The volume-averaged plasma system model (the block in the bottom-left corner of Fig. 1) includes density response models for deuterium (n_D), tritium (n_T), alpha particles (n_α), and impurity particles with atomic number Z_I (n_I):

$$\begin{aligned} \dot{n}_D &= -\frac{n_D}{\tau_D} - S_\alpha + S_D + S^R_D, \quad \dot{n}_\alpha = -\frac{n_\alpha}{\tau_\alpha} + S_\alpha, \\ \dot{n}_T &= -\frac{n_T}{\tau_T} - S_\alpha + S_T + S^R_T, \quad \dot{n}_I = -\frac{n_I}{\tau_I} + S^{sp}_I, \end{aligned} \tag{1}$$

where S_D and S_T are the control inputs ($\mathrm{m^{-3}\,s^{-1}}$). The particle confinement times are τ_α, τ_D, τ_T, and τ_I. The plasma density is $n = n_H + n_\alpha + n_I + n_e$ where $n_H = n_D + n_T$ and the electron density $n_e = n_H + 2n_\alpha + Z_I n_I$ is defined by quasi-neutrality. Using the constants f_{eff}, f_{ref}, R^{eff}, and γ^{PF}, the DT wall-recycling source [6], [19] is modeled as

$$\begin{aligned} S^R_D &= \frac{1}{1-f_{ref}(1-f_{eff})}\left(f_{ref}\frac{n_D}{\tau_D} + \left(\frac{n_D}{\tau_D}+\frac{n_T}{\tau_T}\right)(1-\gamma^{PF})\varphi\right), \\ S^R_T &= \frac{1}{1-f_{ref}(1-f_{eff})}\left(f_{ref}\frac{n_T}{\tau_T} + \left(\frac{n_D}{\tau_D}+\frac{n_T}{\tau_T}\right)\gamma^{PF}\varphi\right), \\ \varphi &= ((1-f_{ref}(1-f_{eff}))R^{eff})(1-R^{eff}(1-f_{eff}))^{-1} - f_{ref}. \end{aligned} \tag{2}$$

Similarly, $S^{sp}_I = f^{sp}_I(n/\tau_I + \dot{n})$ is the impurity sputtering source that depends on the constant f^{sp}_I. The fusion reaction rate density $S_\alpha = n_D n_T \langle\sigma\nu\rangle$ depends on the DT reactivity:

$$\langle\sigma\nu\rangle = C_1 \omega e^{-3\xi}\xi^{\frac{1}{2}}(m_r c^2 T_i^3)^{-\frac{1}{2}}, \quad \xi = (B_G^2/4\omega)^{\frac{1}{3}} \tag{3}$$

where T_i (keV) is the shared temperature of all of the ions. Constants C_1, B_G, and $m_r c^2$ are found in [20] along with ω which is a function of T_i. The tritium fraction is $\gamma = n_T/n_H$.

The total plasma energy is $E = E_i + E_e$ where the ion energy is $E_i = \frac{3}{2}(n_H + n_\alpha + n_I)T_i$, the electron energy is $E_e = \frac{3}{2}n_e T_e$, and the electron temperature is T_e. In this work, T_i and T_e are in J (kinetic energy) unless stated otherwise. The energy response models

$$\begin{aligned} \dot{E}_i &= -\frac{E_i}{\tau_{E,i}} + \phi_\alpha P_\alpha + P_{ei} + P_{aux,i}, \\ \dot{E}_e &= -\frac{E_e}{\tau_{E,e}} + (1-\phi_\alpha)P_\alpha - P_{ei} - P_{br} + P_{oh} + P_{aux,e}, \end{aligned} \tag{4}$$

depend on the ion and electron energy confinement times $\tau_{E,i}$ and $\tau_{E,e}$. The control inputs are $P_{aux,i}$ and $P_{aux,e}$ ($\mathrm{W/m^3}$). Each fusion reaction produces $Q_\alpha = 3.52$ MeV such that the alpha power is $P_\alpha = Q_\alpha S_\alpha$. The bremsstrahlung radiation and the ohmic heating are $P_{br} = 5.5\times10^{-37} Z_{eff} n_e^2 \sqrt{T_e}$ and $P_{oh} = 2.8\times10^{-9} Z_{eff} I_p^2 a^{-4} T_e^{-3/2}$ where T_e is in keV (kinetic energy), I_p is the plasma current, and a is the plasma minor radius. The effective atomic number is $Z_{eff} = (n_H + 4n_\alpha + Z_I^2 n_I)/n_e$. The ion-electron collisional power exchange [21] is

$$P_{ei} = \frac{3}{2} n_e \frac{T_e - T_i}{\tau_{ei}}, \quad \tau_{ei} = \frac{3\pi\sqrt{2\pi}\varepsilon_0^2 T_e^{3/2}}{e^4\sqrt{m_e}\ln\Lambda_e}\sum_l \frac{m_l}{n_l Z_l^2}, \tag{5}$$

where $\varepsilon_0 = 8.854\times10^{-12}$ F/m, m_e is the electron mass (kg), and $e = 1.622\times10^{-19}$ C. With T_k in Kelvin, $\Lambda_k = 1.24\times10^7 T_k^{3/2}/(n_e^{1/2} Z_{eff}^2)$ for $k \in \{i, e\}$. The summation is being taken over the set of plasma ions $l \in \{D, T, \alpha, I\}$, and m_l, n_l, and Z_l refer to the ion mass, density, and atomic number, respectively.

Fusion-born alpha particles and NBI particles heat the plasma's ions and electrons unevenly. Differentiating between alpha and NBI heating, the ion heating fraction is denoted as ϕ_f for $f \in \{\alpha, nbi\}$. In [13], it was shown to be

$$\begin{aligned} \phi_f &= \rho_f \phi^\star_f, \quad \varepsilon_c = \frac{A_f T_e}{m_e^{1/3} n_e^{2/3}}\sum_l \frac{n_l Z_l^2}{A_l}\left(\frac{3\sqrt{\pi}\ln\Lambda_i}{4\ln\Lambda_e}\right)^{2/3}, \\ \phi^\star_f &= \frac{1}{x_0}\left[\frac{1}{3}\ln\frac{1-x_0^{1/2}+x_0}{(1+x_0^{1/2})^2} + \frac{2}{\sqrt{3}}\left(\tan^{-1}\frac{2x_0^{1/2}-1}{\sqrt{3}} + \frac{\pi}{6}\right)\right], \end{aligned} \tag{6}$$

where $x_0 = \varepsilon_{f_0}/\varepsilon_c$, ε_{f_0} is the fast ion's initial energy, A_f

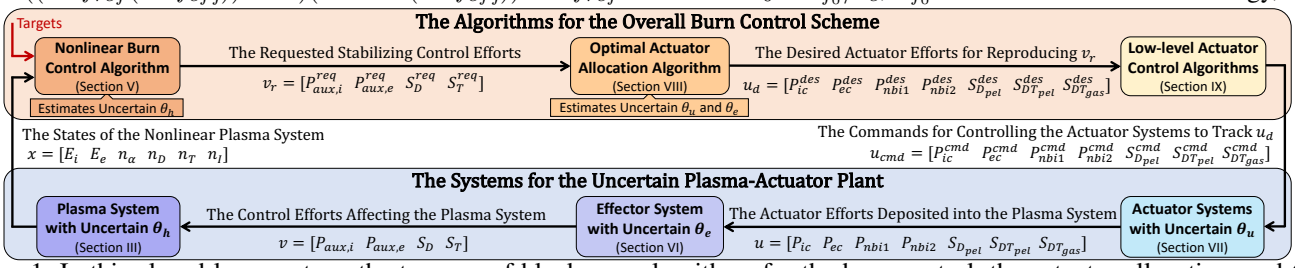

Fig. 1: In this closed-loop system, the top row of blocks are algorithms for the burn control, the actuator allocation, and the low-level actuator control. The bottom row of blocks are the actuator systems, the effector system, and the plasma system.

for $f \in \{\alpha, nbi\}$ is the fast ion's atomic mass, and A_l for $l \in \{D, T, \alpha, I\}$ is the plasma ion's atomic mass [1], [22]. The injected D particles from ITER's NBI ($A_{nbi}=2$) and the fusion alpha particles ($A_\alpha=4$) have $\varepsilon_{nbi_0}=1$ MeV [3] and $\varepsilon_{\alpha_0}=3.52$ MeV of energy. Arbitrary constants ρ_α and ρ_{nbi} are included in (6) so that ϕ_α and ϕ_{nbi} contain uncertainty.

The global energy confinement time [23], [24] is

$$\tau_E \triangleq H\tau_E^{sc} = H\frac{KI_p^{0.93}B_T^{0.15}M^{0.19}R^{1.97}\epsilon^{0.58}\kappa^{0.78}n_{e_{19}}^{0.41}}{P^{0.69}V^{0.69}}, \quad (7)$$

where $K = 0.0562$, H indicates the plasma's confinement quality, V is the plasma volume, R is the plasma major radius, $\epsilon = a/R$, B_T is the toroidal field, $M{=}3\gamma+(1{-}\gamma)$, κ is the vertical elongation at 95% flux surface, $P{=}P_{aux,i}{+}P_{aux,e}{-}P_{br}{+}P_\alpha{+}P_{oh}$ is in MWm^{-3}, and n_e is in 10^{19}m^{-3}. In ITER, I_p, B_T, R, a, κ, and V equal 15 MA, 5.3 T, 6.2 m, 2 m, 1.7, and 837 m^3, respectively. The energy and particle confinement times are proportional to (7): $\tau_{E,i}{=}\zeta_i\tau_E$, $\tau_{E,e}{=}\zeta_e\tau_E$, and $\tau_r{=}k_r\tau_E$ for $r{\in}\{\alpha, D, T, I\}$.

The response models (1) and (4) can be rewritten as

$$\begin{aligned}
\dot{E}_i &= -\theta_{h,1}\frac{E_i}{\tau_E^{sc}} + \theta_{h,3}\phi_\alpha^\star P_\alpha + P_{ei} + P_{aux,i},\\
\dot{E}_e &= -\theta_{h,2}\frac{E_e}{\tau_E^{sc}} + P_\alpha + \theta_{h,4}\phi_\alpha^\star P_\alpha - P_{ei} - P_{br} + P_{oh} + P_{aux,e},\\
\dot{n}_\alpha &= -\theta_{h,5}\frac{n_\alpha}{\tau_E^{sc}} + S_\alpha,\\
\dot{n}_D &= -\theta_{h,6}\frac{n_D}{\tau_E^{sc}} + \theta_{h,9}\frac{n_T}{\tau_E^{sc}} - S_\alpha + S_{D,}\\
\dot{n}_T &= -\theta_{h,7}\frac{n_T}{\tau_E^{sc}} + \theta_{h,10}\frac{n_D}{\tau_E^{sc}} - S_\alpha + S_T,\\
\dot{n}_I &= -\theta_{h,8}\frac{n_I}{\tau_E^{sc}} + \theta_{h,11}\frac{n}{\tau_E^{sc}} + \theta_{h,12}\dot{n},
\end{aligned} \quad (8)$$

where the elements of $\theta_h^T = [\theta_{h,1}\ \theta_{h,2}\ \ldots\ \theta_{h,12}]$ lump together the following parameters which are uncertain: H, ζ_i, ζ_e, k_D, k_T, k_α, k_I, f_{eff}, f_{ref}, R^{eff}, γ^{PF}, f_I^{sp}, and ρ_α. With (1), (4), and (8), the elements of θ_h can be readily inferred.

IV. BURN CONTROL OBJECTIVES

The vector $x \triangleq [E_i\ E_e\ n_\alpha\ n_D\ n_T\ n_I]^T$ contains the states of system (8). With six desired values for the states ($\bar{x}$) and four control efforts ($\bar{P}_{aux,i}$, $\bar{P}_{aux,e}$, $\bar{S}_D$, $\bar{S}_T$), the six equations (8) at steady-state ($d/dt{=}0$) can be solved by choosing $\bar{E}_i$, $\bar{E}_e$, $\bar{n}$, and $\bar{\gamma}$. The burn control objective is to drive the following system to the origin (i.e., $\tilde{x}{=}x{-}\bar{x}{\to}0$):

$$\begin{aligned}
\dot{\tilde{E}}_i &= -\theta_{h,1}\frac{\bar{E}_i+\tilde{E}_i}{\tau_E^{sc}} + \theta_{h,3}\phi_\alpha^\star P_\alpha + P_{ei} + P_{aux,i},\\
\dot{\tilde{E}}_e &= -\theta_{h,2}\frac{\bar{E}_e+\tilde{E}_e}{\tau_E^{sc}} + P_\alpha + \theta_{h,4}\phi_\alpha^\star P_\alpha - P_{ei} - P_{br} + P_{oh} + P_{aux,e},\\
\dot{\tilde{n}}_\alpha &= -\theta_{h,5}\frac{\bar{n}_\alpha+\tilde{n}_\alpha}{\tau_E^{sc}} + S_\alpha,\\
\dot{\tilde{n}}_D &= -\theta_{h,6}\frac{\bar{n}_D+\tilde{n}_D}{\tau_E^{sc}} + \theta_{h,9}\frac{\bar{n}_T+\tilde{n}_T}{\tau_E^{sc}} - S_\alpha + S_D,\\
\dot{\tilde{n}}_T &= -\theta_{h,7}\frac{\bar{n}_T+\tilde{n}_T}{\tau_E^{sc}} + \theta_{h,10}\frac{\bar{n}_D+\tilde{n}_D}{\tau_E^{sc}} - S_\alpha + S_T,\\
\dot{\tilde{n}}_I &= -\theta_{h,8}\frac{\bar{n}_I+\tilde{n}_I}{\tau_E^{sc}} + \theta_{h,11}\frac{\bar{n}+\tilde{n}}{\tau_E^{sc}} + \theta_{h,12}\dot{\tilde{n}}.
\end{aligned} \quad (9)$$

V. NONLINEAR BURN CONTROL

The control laws for the burn control algorithm (the leftmost block on the top row in Fig. 1) are designed with the following Lyapunov function and its time derivative [15]:

$$\begin{aligned}
V &= w_i^2\tilde{E}_i^2 + w_e^2\tilde{E}_e^2 + w_\gamma^2\tilde{\gamma}^2 + \tilde{n}^2 + \tilde{\theta}_h^T\Gamma_h^{-1}\tilde{\theta}_h,\\
\dot{V} &= w_i^2\tilde{E}_i\dot{\tilde{E}}_i + w_e^2\tilde{E}_e\dot{\tilde{E}}_e + w_\gamma^2\tilde{\gamma}\dot{\tilde{\gamma}} + \tilde{n}\dot{\tilde{n}} + \tilde{\theta}_h^T\Gamma_h^{-1}\dot{\tilde{\theta}}_h,
\end{aligned} \quad (10)$$

where Γ_h is a positive definite matrix, and w_i, w_e, and w_γ are positive constants. Since θ_h is uncertain (not known), the controller's estimate of it $\hat{\theta}_h$ will have the error $\tilde{\theta}_h{=}\hat{\theta}_h{-}\theta_h$.

The expressions for $\tilde{E}_i$ and $\tilde{E}_e$ from (9) can be immediately substituted into $\dot{V}$ (10). Expression for $\dot{\tilde{n}}$ and $\dot{\tilde{\gamma}}$ [14] can be found using (9), $n_H{=}n_D+n_T$, $n{=}n_H{+}n_\alpha{+}n_I{+}n_e$, $n_e{=}n_H{+}2n_\alpha{+}Z_In_I$, $\gamma{=}n_T/n_H$, and differentiation:

$$\begin{aligned}
\dot{\tilde{n}} &= 2S_D + 2S_T - 3\theta_{h,5}\frac{n_\alpha}{\tau_E^{sc}} - 2\theta_{h,6}\frac{n_D}{\tau_E^{sc}} - 2\theta_{h,7}\frac{n_T}{\tau_E^{sc}} + 2\theta_{h,9}\frac{n_T}{\tau_E^{sc}}\\
&\quad + 2\theta_{h,10}\frac{n_D}{\tau_E^{sc}} - S_\alpha + (Z_I+1)\left(\theta_{h,11}\frac{n}{\tau_E^{sc}} + \theta_{h,12}\dot{n} - \theta_{h,8}\frac{n_I}{\tau_E^{sc}}\right),\\
\dot{\tilde{\gamma}} &= \frac{1}{n_H}\Bigg[-\theta_{h,7}\frac{n_T}{\tau_E^{sc}} - S_\alpha + S_T + \theta_{h,10}\frac{n_D}{\tau_E^{sc}} - \gamma\left(-\theta_{h,7}\frac{n_T}{\tau_E^{sc}}\right.\\
&\quad \left.-\theta_{h,6}\frac{n_D}{\tau_E^{sc}} - 2S_\alpha + S_D + S_T + \theta_{h,9}\frac{n_T}{\tau_E^{sc}} + \theta_{h,10}\frac{n_D}{\tau_E^{sc}}\right)\Bigg].
\end{aligned} \quad (11)$$

Substituting the $\dot{\tilde{E}}_i$, $\dot{\tilde{E}}_e$, $\dot{\tilde{n}}$ and $\dot{\tilde{\gamma}}$ expressions into (10) gives

$$\begin{aligned}
\dot{V} &= w_i^2\tilde{E}_i\left[P_{aux,i} - \theta_{h,1}\left(\frac{\bar{E}_i+\tilde{E}_i}{\tau_E^{sc}}\right) + \theta_{h,3}\phi_\alpha^\star P_\alpha + P_{ei}\right] + \tilde{\theta}_h^T\Gamma_h^{-1}\dot{\tilde{\theta}}_h\\
&\quad + w_e^2\tilde{E}_e\left[P_{aux,e} - \theta_{h,2}\left(\frac{\bar{E}_e+\tilde{E}_e}{\tau_E^{sc}}\right) + \theta_{h,4}\phi_\alpha^\star P_\alpha + P_\alpha - P_{ei} - P_{br}\right.\\
&\quad \left. + P_{oh}\right] + \frac{w_\gamma^2\tilde{\gamma}}{n_H}\left[\theta_{h,10}\frac{n_D}{\tau_E^{sc}} - \theta_{h,7}\frac{n_T}{\tau_E^{sc}} - S_\alpha + S_T - \gamma\left(S_D + S_T\right.\right.\\
&\quad \left.\left. + \frac{n_T}{\tau_E^{sc}}\left(\theta_{h,9} - \theta_{h,7}\right) + \frac{n_D}{\tau_E^{sc}}\left(\theta_{h,10} - \theta_{h,6}\right) - 2S_\alpha\right)\right] + \tilde{n}\left[2S_D - S_\alpha\right.\\
&\quad \left. - 2\theta_{h,7}\frac{n_T}{\tau_E^{sc}} + (Z_I+1)\left(\theta_{h,11}\frac{n}{\tau_E^{sc}} + \theta_{h,12}\dot{n} - \theta_{h,8}\frac{n_I}{\tau_E^{sc}}\right) + 2S_T\right.\\
&\quad \left. - 2\theta_{h,6}\frac{n_D}{\tau_E^{sc}} + 2\theta_{h,9}\frac{n_T}{\tau_E^{sc}} + 2\theta_{h,10}\frac{n_D}{\tau_E^{sc}} - 3\theta_{h,5}\frac{n_\alpha}{\tau_E^{sc}}\right].
\end{aligned} \quad (12)$$

Using the certainty equivalence principle where $\hat{\theta}_h{=}\theta_h$ is temporarily assumed [25], the control laws are formulated:

$$\begin{aligned}
P_{aux,i}^{req} &= \hat{\theta}_{h,1}\frac{\bar{E}_i}{\tau_E^{sc}} - \hat{\theta}_{h,3}\phi_\alpha^\star P_\alpha - P_{ei},\\
P_{aux,e}^{req} &= \hat{\theta}_{h,2}\frac{\bar{E}_e}{\tau_E^{sc}} - P_\alpha - \hat{\theta}_{h,4}\phi_\alpha^\star P_\alpha + P_{ei} + P_{br} - P_{oh},\\
S_D^{req} &= \frac{n_D}{\tau_E^{sc}}\left(\hat{\theta}_{h,6} - \hat{\theta}_{h,10}\right) + \frac{n_T}{\tau_E^{sc}}\left(\hat{\theta}_{h,7} - \hat{\theta}_{h,9}\right) - S_T + \frac{1}{2}\left[3\hat{\theta}_{h,5}\frac{n_\alpha}{\tau_E^{sc}}\right.\\
&\quad \left. + (Z_I+1)\left(\hat{\theta}_{h,8}\frac{n_I}{\tau_E^{sc}} - \hat{\theta}_{h,11}\frac{n}{\tau_E^{sc}} - \hat{\theta}_{h,12}\dot{n}\right) + S_\alpha - \mu_n\tilde{n}\right],\\
S_T^{req} &= \hat{\theta}_{h,7}\frac{n_T}{\tau_E^{sc}} + S_\alpha - \hat{\theta}_{h,10}\frac{n_D}{\tau_E^{sc}} - \mu_t\tilde{\gamma} + \frac{\gamma}{2}\left[3\hat{\theta}_{h,5}\frac{n_\alpha}{\tau_E^{sc}} - 3S_\alpha\right.\\
&\quad \left. + (Z_I+1)\left(\hat{\theta}_{h,8}\frac{n_I}{\tau_E^{sc}} - \hat{\theta}_{h,11}\frac{n}{\tau_E^{sc}} - \hat{\theta}_{h,12}\dot{n}\right) - \mu_n\tilde{n}\right],
\end{aligned} \quad (13)$$

where μ_n and μ_t are positive constants. Substitution of the four control laws (13) into $\dot{V}$ (12) gives the following result:

$$\dot{V} = w_i^2\tilde{E}_i\frac{\bar{E}_i}{\tau_E^{sc}}\tilde{\theta}_{h,1} + w_e^2\tilde{E}_e\frac{\bar{E}_e}{\tau_E^{sc}}\tilde{\theta}_{h,2} - \frac{w_i^2\tilde{E}_i^2}{\tau_E^{sc}}\theta_{h,1} - \frac{w_e^2\tilde{E}_e^2}{\tau_E^{sc}}\theta_{h,2}$$
$$- w_i^2\tilde{E}_i P_\alpha\phi_\alpha^\star\tilde{\theta}_{h,3} - w_e^2\tilde{E}_e P_\alpha\phi_\alpha^\star\tilde{\theta}_{h,4} + 3\tilde{n}\frac{n_\alpha}{\tau_E^{sc}}\tilde{\theta}_{h,5} - \mu_t\frac{w_\gamma^2\tilde{\gamma}^2}{n_H}$$
$$+ \left(2\tilde{n} - \frac{w_\gamma^2\tilde{\gamma}\gamma}{n_H}\right)\frac{n_D}{\tau_E^{sc}}\tilde{\theta}_{h,6} + \left(2\tilde{n} - (\gamma-1)\frac{w_\gamma^2\tilde{\gamma}}{n_H}\right)\frac{n_T}{\tau_E^{sc}}\tilde{\theta}_{h,7} - \mu_n\tilde{n}^2$$
$$+ \tilde{n}(Z_I+1)\frac{n_I}{\tau_E^{sc}}\tilde{\theta}_{h,8} + \left(\frac{w_\gamma^2\tilde{\gamma}\gamma}{n_H} - 2\tilde{n}\right)\frac{n_T}{\tau_E^{sc}}\tilde{\theta}_{h,9} - (Z_I+1)\tilde{n}\dot{n}\tilde{\theta}_{h,12}$$
$$+ (\gamma-1)\frac{w_\gamma^2\tilde{\gamma}n_D}{n_H\tau_E^{sc}}\tilde{\theta}_{h,10} - \tilde{n}(Z_I+1)\frac{n}{\tau_E^{sc}}\tilde{\theta}_{h,11} + \tilde{\theta}_h^T\Gamma_h^{-1}\dot{\tilde{\theta}}_h. \quad (14)$$

Because the assumption that $\hat{\theta}_h = \theta_h$ (i.e., $\tilde{\theta}_h = 0$) will not always hold, the following adaptive estimation law is chosen to eliminate the terms that contain the elements of $\tilde{\theta}_h$ in (14):

$$\dot{\hat{\theta}}_h \approx \dot{\tilde{\theta}}_h = \Gamma_h \begin{bmatrix} -(\bar{E}_i/\tau_E^{sc})w_i^2\tilde{E}_i \\ -(\bar{E}_e/\tau_E^{sc})w_e^2\tilde{E}_e \\ \phi_\alpha^\star P_\alpha w_i^2\tilde{E}_i \\ \phi_\alpha^\star P_\alpha w_e^2\tilde{E}_e \\ -3\tilde{n}(n_\alpha/\tau_E^{sc}) \\ -[2\tilde{n} - ((w_\gamma^2\tilde{\gamma}\gamma)/n_H)](n_D/\tau_E^{sc}) \\ -[2\tilde{n} - (\gamma-1)(w_\gamma^2\tilde{\gamma})/n_H](n_T/\tau_E^{sc}) \\ -\tilde{n}(Z_I+1)(n_I/\tau_E^{sc}) \\ -(((w_\gamma^2\tilde{\gamma})/n_H)\gamma - 2\tilde{n})(n_T/\tau_E^{sc}) \\ -(\gamma-1)((w_\gamma^2\tilde{\gamma})/n_H)(n_D/\tau_E^{sc}) \\ \tilde{n}(Z_I+1)(n/\tau_E^{sc}) \\ (Z_I+1)\tilde{n}\dot{n} \end{bmatrix}. \quad (15)$$

The $\dot{\hat{\theta}}_h \approx \dot{\tilde{\theta}}_h$ condition holds because variations in the uncertain parameters are assumed to be slow ($\dot{\theta}_h \approx 0$).

Substituting (15) into (14) gives the stability condition

$$\dot{V} = -\frac{w_i^2\tilde{E}_i^2}{\tau_E^{sc}}\theta_{h,1} - \frac{w_e^2\tilde{E}_e^2}{\tau_E^{sc}}\theta_{h,2} - \mu_t\frac{w_\gamma^2\tilde{\gamma}^2}{n_H} - \mu_n\tilde{n}^2 \le 0, \quad (16)$$

which holds because τ_E^{sc}, $\theta_{h,1}$, $\theta_{h,2}$, and n_H are positive. It is not guaranteed that the estimation errors in $\tilde{\theta}_h$ are forced to zero. In the state space ($\tilde{E}_i$, $\tilde{E}_e$, $\tilde{\gamma}$, $\tilde{n}$, $\tilde{\theta}_h$), the set Ω is defined by all points where $\dot{V} = 0$. From (16), it is clear that $\dot{V} = 0$ only when $\tilde{E}_i$, $\tilde{E}_e$, $\tilde{\gamma}$, and $\tilde{n}$ are equal to zero (irrespective of the value of $\tilde{\theta}_h$). Therefore by LaSalle's Theorem [15], the deviations $\tilde{E}_i$, $\tilde{E}_e$, $\tilde{\gamma}$, and $\tilde{n}$ are driven to zero as $t \to \infty$.

The following shows that $\tilde{n}_\alpha$ and $\tilde{n}_I$ are driven to zero. With (8), the time derivative of the Lyapunov function $V_\alpha = \tilde{n}_\alpha^2/2$ is $\dot{V}_\alpha = \tilde{n}_\alpha(S_\alpha - \theta_{h,5}n_\alpha/\tau_E^{sc})$. With $\tilde{E}_i$, $\tilde{E}_e$, $\tilde{\gamma}$, and $\tilde{n}$ driven to zero, the expression $(S_\alpha - \theta_{h,5}n_\alpha/\tau_E^{sc})$ decreases with increasing n_α and vice versa. Therefore, the statement $S_\alpha - \theta_{h,5}n_\alpha/\tau_E^{sc} = -\vartheta\tilde{n}_\alpha$ holds if ϑ is a positive continuous function. When $\tilde{E}_i$, $\tilde{E}_e$, $\tilde{\gamma}$, and $\tilde{n}$ equal zero, $\dot{V}_\alpha = -\vartheta\tilde{n}_\alpha^2 < 0 \ \forall \ \tilde{n}_\alpha \neq 0$. Therefore, $\tilde{n}_\alpha \to 0$ over time. With $S_I^{sp} = f_I^{sp}(n/\tau_I + \dot{n})$, the n_I response model (1) reduces to $0 = -n_I + f_I^{sp}n$ at steady-state. When $\tilde{n} = 0$, it can be seen that $\tilde{n}_I = 0$. Clearly, driving $\tilde{n}$ to zero brings $\tilde{n}_I$ to zero.

VI. THE EFFECTOR SYSTEM

To satisfy the control laws (13), ITER will have access to various actuators that output actuator efforts $u \triangleq [P_{ic}\ P_{ec}\ P_{nbi_1}\ P_{nbi_2}\ S_{D_{pel}}\ S_{DT_{pel}}\ S_{DT_{gas}}]^T$. Unlike prior work [14], this work includes gas injection. The model of the effector system (the bottom-middle block in Fig. 1) maps the control efforts $v \triangleq [P_{aux,i}\ P_{aux,e}\ S_D\ S_T]^T = \Phi(x,u)$ to u:

$$P_{aux,i} = \eta_{ic}P_{ic} + \eta_{nbi_1}\phi_{nbi}P_{nbi_1} + \eta_{nbi_2}\phi_{nbi}P_{nbi_2},$$
$$P_{aux,e} = \eta_{ec}P_{ec} + \eta_{nbi_1}\bar{\phi}_{nbi}P_{nbi_1} + \eta_{nbi_2}\bar{\phi}_{nbi}P_{nbi_2},$$
$$S_D = \eta_{nbi_1}P_{nbi_1}/\varepsilon_{nbi_0} + \eta_{nbi_2}P_{nbi_2}/\varepsilon_{nbi_0} + \eta_{pel_1}S_{D_{pel}}$$
$$+ \eta_{pel_2}(1-\gamma_{pel})S_{DT_{pel}} + \eta_{gas}(1-\gamma_{gas})S_{DT_{gas}},$$
$$S_T = \eta_{pel_2}\gamma_{pel}S_{DT_{pel}} + \eta_{gas}\gamma_{gas}S_{DT_{gas}}, \quad (17)$$

where η_{ic}, η_{ec}, η_{nbi_1}, η_{nbi_2}, η_{pel_1}, η_{pel_2}, and η_{gas} are uncertain efficiency factors. The ion cyclotron (IC) and electron cyclotron (EC) systems provide powers P_{ic} and P_{ec} to the ions and electrons, respectively. Through particle collisions (P_{ei} in (4)), they heat the entire plasma. The two neutral beam injectors (NBI) output powers P_{nbi_1} and P_{nbi_2}. The fraction ϕ_{nbi} (6) of the NBI power is deposited into the ions, while the electrons receive $\bar{\phi}_{nbi} = 1 - \phi_{nbi}$. In contrast to prior work [14], this work considers the fueling from NBI. Because ITER's NBI will fire $\varepsilon_{nbi_0} = 1$ MeV D particles [3], the NBI fueling rate is the NBI power divided by ε_{nbi_0}. The 100% D pellet injector fuels at a rate of $S_{D_{pel}}$. Using pellets with a T concentration of γ_{pel}, the DT pellet injector fuels at a rate of $S_{DT_{pel}}$. The gas fueling system puffs gas with a T concentration of γ_{gas} at the rate $S_{DT_{gas}}$. Similarly to [26], the T concentrations (γ_{pel}, γ_{gas}) are uncertain parameters.

In the effector system model (17), some of the uncertain parameters that were constant in prior work [14] are time-varying in this work. The dependence of ϕ_{nbi} on the plasma state is given by (6) which includes the uncertain parameter ρ_{nbi}. The pellet fueling efficiency decreases with increasing plasma energy. This is modeled in an ad-hoc fashion:

$$\eta_{pel_1} = \rho_{pel_1}E_{norm}, \qquad \eta_{pel_2} = \rho_{pel_2}E_{norm}, \quad (18)$$

where $E_{norm} = 1 - E/E_0$ and $E_0 > E = E_i + E_e$ is a constant design parameter that is given in Section X. The arbitrary constants ρ_{pel_1} and ρ_{pel_2} are considered to be uncertain.

VII. THE DYNAMIC ACTUATOR SYSTEMS

ITER's actuators will experience lags such as the NBI thermalization delay and the flight time of the pellets [27]. In (17), u contains the actuator efforts after they been delayed. The commands that are instantaneously sent to the actuators are $u_{cmd} \triangleq [P_{ic}^{cmd}\ P_{ec}^{cmd}\ \dots\ S_{DT_{gas}}^{cmd}]^T$. Each actuator undergoes the same first-order lag process:

$$T_{lag}\dot{u} + u = u_{cmd}, \quad (19)$$

where $T_{lag} = \text{diag}(\tau_{ic}^{lag}, \tau_{ec}^{lag}, \tau_{nbi}^{lag}, \tau_{nbi}^{lag}, \tau_{pel}^{lag}, \tau_{pel}^{lag}, \tau_{gas}^{lag})$ contains the uncertain time constants for the actuators. In contrast to prior work [14], the NBI time constant τ_{nbi}^{lag} is time-varying. NBI particles lose energy at a rate of [1], [21]:

$$\frac{d\varepsilon_{nbi}}{dt} = -B\varepsilon_{nbi} - B\varepsilon_{nbi}\left(\varepsilon_c/\varepsilon_{nbi}\right)^{3/2}, \quad (20)$$

where $B = e^4 n_e m_e^{1/2}\ln\Lambda_e/(3\sqrt{2}\pi^{3/2}\varepsilon_0^2 m_{nbi}T_e^{3/2})$ and $m_{nbi} = 3.343\times10^{-27}$ kg. With the particles' thermalized energy being $\varepsilon_{nbi_{th}} = T_i$, the NBI thermalization delay is found by integrating (20) from zero to the thermalization time:

$$\tau_{nbi}^{lag} = \rho_{th}\tau_{nbi}^\star = -\rho_{th}\frac{2}{3B}\ln\left[\frac{(\frac{\varepsilon_{nbi_{th}}}{\varepsilon_{nbi_0}})^{3/2} + (\frac{\varepsilon_c}{\varepsilon_{nbi_0}})^{3/2}}{1 + (\frac{\varepsilon_c}{\varepsilon_{nbi_0}})^{3/2}}\right], \quad (21)$$

where ρ_{th} is a proportionality constant that is considered to be uncertain and ε_c is given in (6). In Fig. 1, the rightmost block on the bottom row depicts the actuator systems (19).

VIII. OPTIMAL ACTUATOR ALLOCATION

To formulate the actuator allocation algorithm (the top-middle block in Fig. 1), the models for the plasma (8), effector (17), and actuator (19) systems are restructured [18]. The plasma system model can be written as $\dot{x}=f(x)+g(x)v$ where $x=[E_i\ E_e\ n_\alpha\ n_D\ n_T\ n_I]^T$. Both $f(x)$ and $g(x)$ can be easily inferred. The remaining models can be rewritten as

$$\begin{aligned}
&v=\Phi(x,u,\theta_e)=\Phi_{\theta_e}(x,u)\theta_e, \qquad \dot{u}=f_{\theta_u}(x,u,u_{cmd})\theta_u,\\
&\theta_u^T=\begin{bmatrix}1/\tau_{ic}^{lag} & 1/\tau_{ec}^{lag} & 1/\rho_{th} & 1/\tau_{pel}^{lag} & 1/\tau_{gas}^{lag}\end{bmatrix},\\
&\theta_{e_1}^T=\begin{bmatrix}\eta_{ic} & \eta_{nbi_1}\rho_{nbi} & \eta_{nbi_2}\rho_{nbi} & \eta_{ec} & \eta_{nbi_1} & \eta_{nbi_2}\end{bmatrix},\\
&\theta_{e_2}^T=\begin{bmatrix}\rho_{pel_1} & \rho_{pel_2} & \rho_{pel_2}\gamma_{pel} & \eta_{gas} & \eta_{gas}\gamma_{gas}\end{bmatrix},
\end{aligned} \tag{22}$$

where $\theta_e^T=[\theta_{e_1}\ \theta_{e_2}]$. The rewritten models for the effector system (17) and the dynamic actuator systems (19) are, respectively, $v=[P_{aux,i}\ P_{aux,e}\ S_D\ S_T]^T=\Phi=\Phi_{\theta_e}\theta_e$ and $\dot{u}=[\dot{P}_{ic}\ \dot{P}_{ec}\ \dots\ \dot{S}_{DT_{gas}}]^T=f_{\theta_u}\theta_u$. The estimates of θ_e and θ_u, which lump together the uncertain parameters, are $\hat{\theta}_e$ and $\hat{\theta}_u$. Matrices $\Phi(x,u,\theta_e)$, $\Phi_{\theta_e}(x,u)$, and $f_{\theta_u}(x,u,u_{cmd})$ can be inferred by comparing (22) to (17) and (19).

The actuator allocation algorithm seeks to minimize the difference between the requested control efforts v_r (13) and the control efforts that are produced by the actuators v (17) by determining the optimal or desired actuator efforts u_d. It is based on the following constrained optimization problem:

$$\begin{aligned}
&\underset{u_d}{\text{minimize}}\ J=z(\text{diag}(u_d)u_d)-\sum_{i=1}^{i=7}q_i\log(\bar{u}_i-u_{d,i})\\
&\text{subject to}\ v_r-\Phi(x,u_d+\tilde{u},\hat{\theta}_e)=0,
\end{aligned} \tag{23}$$

where $\tilde{u}=u-u_d$ and $u_{d,i}$ is the i^{th} element of u_d. Vector $\bar{u}=[\bar{P}_{ic}\ \bar{P}_{ec}\ \dots\ \bar{S}_{DT_{gas}}]^T$ contains the saturation limits of ITER's actuators [2], [28]: $\bar{u}=[20\,\text{MW}\quad 20\,\text{MW}\quad 16.5\,\text{MW}\quad 16.5\,\text{MW}\quad 120\,\text{Pa}\,\text{m}^3/\text{s}\quad 111\,\text{Pa}\,\text{m}^3/\text{s}\quad 400\,\text{Pa}\,\text{m}^3/\text{s}]^T$. The vectors z and q consist of weighting constants. With the introduction of a Lagrangian function L and vector λ, (23) can be rewritten as an unconstrained optimization problem:

$$\begin{aligned}
&\underset{u_d,\lambda}{\text{minimize}}\ L(x,u_d,\tilde{u},\lambda,\hat{\theta}_e,\hat{\theta}_u),\\
&L(x,u_d,\tilde{u},\lambda,\hat{\theta}_e,\hat{\theta}_u)=J+(v_r-\Phi(x,u_d+\tilde{u},\hat{\theta}_e))^T\lambda.
\end{aligned} \tag{24}$$

The allocation algorithm makes use of two observers:

$$\begin{aligned}
\dot{\hat{u}}&=A_{\hat{u}}(\hat{u}-u)+f_{\theta_u}(x,u,u_{cmd})\hat{\theta}_u,\\
\dot{\hat{x}}&=A_{\hat{x}}(\hat{x}-x)+f(x)+g(x)\Phi(x,u,\hat{\theta}_e),
\end{aligned} \tag{25}$$

where $A_{\hat{u}}$ and $A_{\hat{x}}$ are Hurwitz matrices. The update laws for the actuator allocation are based on the formulation in [18]:

$$\begin{aligned}
&\begin{pmatrix}\dot{u}_d\\ \dot{\lambda}\end{pmatrix}=-\Gamma H\begin{pmatrix}\frac{\partial L}{\partial u_d}\\ \frac{\partial L}{\partial \lambda}\end{pmatrix}-u_{ff},\quad H=\begin{pmatrix}\frac{\partial^2 L}{\partial u_d^2} & \frac{\partial^2 L}{\partial\lambda\partial u_d}\\ \frac{\partial^2 L}{\partial u_d\partial\lambda} & 0\end{pmatrix},\\
&u_{ff}=H^{-1}\begin{pmatrix}\frac{\partial^2 L}{\partial\tilde{u}\partial u_d}\\ \frac{\partial^2 L}{\partial\tilde{u}\partial\lambda}\end{pmatrix}f_{\tilde{u}}(x,\tilde{u},u_d,u_{cmd},\hat{\theta}_u)+H^{-1}\begin{pmatrix}\frac{\partial^2 L}{\partial\hat{\theta}\partial u_d}\\ \frac{\partial^2 L}{\partial\hat{\theta}\partial\lambda}\end{pmatrix}\dot{\hat{\theta}}\\
&\qquad +H^{-1}\left(\begin{pmatrix}\frac{\partial^2 L}{\partial x\partial u_d}\\ \frac{\partial^2 L}{\partial x\partial\lambda}\end{pmatrix}(f(x)+g(x)(v_r-\Phi(x,u,\theta_e)))\right),\\
&\dot{\hat{\theta}}_u^T=\left(\xi_u^T\Gamma_u+\xi_x^T\Gamma_x+\frac{\partial V_{\tilde{u}}}{\partial\tilde{u}}+\frac{\partial L^T}{\partial u_d}\frac{\partial^2 L}{\partial\tilde{u}\partial u_d}+\frac{\partial L^T}{\partial\lambda}\frac{\partial^2 L}{\partial\tilde{u}\partial\lambda}\right)f_{\theta_u}\Gamma_{\theta_u}^{-1},\\
&\dot{\hat{\theta}}_e^T=\left(\xi_x^T\Gamma_x+\frac{\partial L^T}{\partial\lambda}\frac{\partial^2 L}{\partial x\partial\lambda}\right)g(x)\Phi_{\theta_e}(x,u)\Gamma_{\theta_e}^{-1},
\end{aligned} \tag{26}$$

where $\hat{\theta}\triangleq(\hat{\theta}_u^T,\hat{\theta}_e^T)^T$, $\xi_u\triangleq u-\hat{u}$, $\xi_x\triangleq x-\hat{x}$. The matrices Γ, Γ_{θ_u}, Γ_{θ_e}, Γ_u, and Γ_x are symmetric and positive definite.

IX. LOW-LEVEL ACTUATOR CONTROL

Because of the actuator dynamics (19), low-level actuator control algorithms (the top-right block in Fig. 1) give commands u_{cmd} to bring the actuator efforts u to the desired u_d. Their control laws are designed with the Lyapunov functions:

$$V_{\tilde{u},i}=\tilde{u}_i^2/2\quad\text{for}\quad i\in\{1,...,7\}, \tag{27}$$

where each $V_{\tilde{u},i}$ is a function of the i^{th} element of $\tilde{u}=[\tilde{P}_{ic}\ \tilde{P}_{ec}\ \tilde{P}_{nbi_1}\ \tilde{P}_{nbi_2}\ \tilde{S}_{D_{pel}}\ \tilde{S}_{DT_{pel}}\ \tilde{S}_{DT_{gas}}]^T=u-u_d$.

The models for the actuator systems (19) are rewritten as

$$\begin{aligned}
&\dot{u}_i=\Theta_{u,i}(u_{cmd,i}-u_i)\quad\text{for}\quad i\in\{1,...,7\},\\
&\Theta_u^T=[\theta_{u,1}\ \ \theta_{u,2}\ \ \theta_{u,3}/\tau_{nbi}^{\star}\ \ \theta_{u,3}/\tau_{nbi}^{\star}\ \ \theta_{u,4}\ \ \theta_{u,4}\ \ \theta_{u,5}],
\end{aligned} \tag{28}$$

where $u_{cmd,i}$, $\Theta_{u,i}$, and $\theta_{u,i}$ indicate the i^{th} element of u_{cmd}, Θ_u from (28), and θ_u from (22), respectively. Taking the time derivative of $V_{\tilde{u},i}$ (27) and substituting for $\tilde{u}_i=u_i-u_{d,i}$ gives

$$\dot{V}_{\tilde{u},i}=\tilde{u}_i\dot{\tilde{u}}_i=\tilde{u}_i(\Theta_{u,i}(u_{cmd,i}-\tilde{u}_i-u_{d,i})-\dot{u}_{d,i}), \tag{29}$$

for $i\in\{1,...,7\}$. The low-level actuator control algorithms assume that $\hat{\Theta}_u=\Theta_u$ where $\hat{\Theta}_u$ is the actuator allocation algorithm's estimate of Θ_u (i.e., $\hat{\Theta}_u=[\hat{\theta}_{u,1}\ \hat{\theta}_{u,2}\ \dots\ \hat{\theta}_{u,5}]^T$). With the control laws (and for $\hat{\Theta}_u=\Theta_u$ and $\Theta_{u,i}>0$),

$$u_{cmd,i}=u_{d,i}+\dot{u}_{d,i}/\hat{\Theta}_{u,i}\quad\text{for}\quad i\in\{1,...,7\}, \tag{30}$$

the stability condition $\dot{V}_{\tilde{u},i}=-\tilde{u}_i^2\hat{\Theta}_{u,i}<0\ \ \forall\,\tilde{u}_i\neq 0$ is met.

In tokamaks, various controllers with different objectives may compete over the actuators. Therefore, some of the actuators in (17) may not always be available to the presented burn control scheme (Sections V through IX). As evidenced by the prior work [14] where the gas fueling system was not included, the actuator allocation algorithm (22)−(26) can be reformulated to include more or less actuators. Therefore, the presented burn control scheme can be used as a component of a high-level management system [10], [11] that swaps in and out different versions of the presented actuator allocation algorithm as needed. The advantage of the presented burn control scheme is that it can deal with actuation lags and uncertainties in the plasma, effector and actuator systems. The presented burn control scheme decouples the burn control problem from the actuator allocation problem. This results in a modular design that allows the burn control algorithm to be swapped with different controllers or the actuator allocation algorithm to be swapped with different allocators.

X. SIMULATION STUDY

The burn control scheme (Sections V through IX) is tested in a simulation with initial conditions: $n_\alpha=2\times10^{18}\text{m}^{-3}$, $n_D=3\times10^{19}\text{m}^{-3}$, $n_T=3\times10^{19}\text{m}^{-3}$, $n_I=1\times10^{18}\text{m}^{-3}$, $E_i=1.4\times10^5\text{J/m}^3$, and $E_e=1.8\times10^5\text{J/m}^3$. The first target for burn control was the solution of (8) with $d/dt=0$ when $\bar{E}_i=1.3\times10^5\text{J/m}^3$, $\bar{E}_e=1.9\times10^5\text{J/m}^3$, $\bar{n}=1.5\times10^{20}\text{m}^{-3}$, and $\bar{\gamma}=0.5$. After 100 s, the target changed to solution when $\bar{E}_i=1.2\times10^5\text{J/m}^3$, $\bar{E}_e=1.8\times10^5\text{J/m}^3$, $\bar{n}=1.4\times10^{20}\text{m}^{-3}$, and $\bar{\gamma}=0.5$. In addition, $Z_I=4$ and $E_0=5.9\times10^5$ J/m^{-3}.

Respectively, the uncertain parameters for the plasma system model $H,\zeta_i,\zeta_e,k_D,k_T,k_\alpha,k_I,\rho_\alpha,f_{eff},f_{ref},R^{eff}$, γ^{PF}, and f_I^{sp} were given the following values: $1, 1.1, 0.9, 3, 2, 4, 6, 1, 0.1, 0.5, 0.6, 0.5$, and 0.01. The values for the recycling parameters are within range of that reported in [19]. For the effector system model, the uncertain parameters η_{ic},η_{ec},

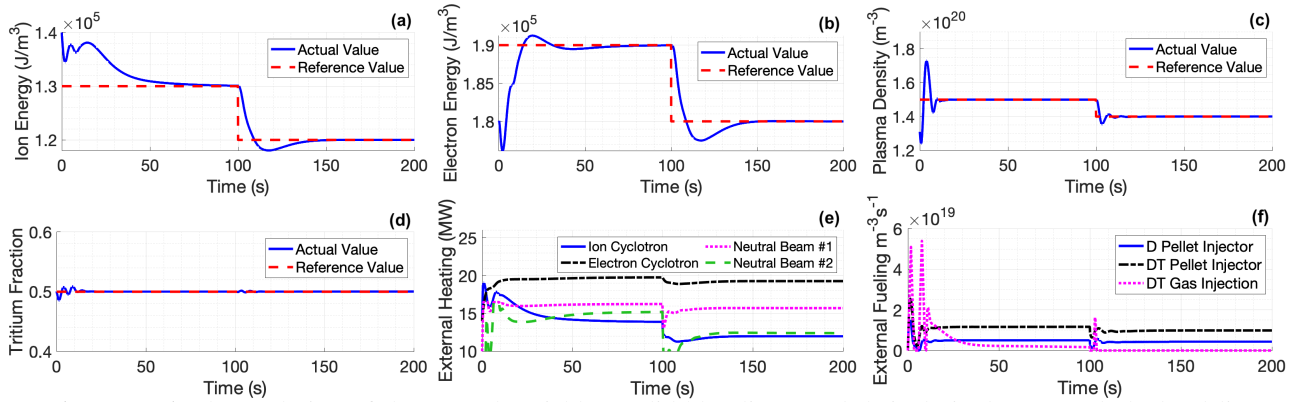

Fig. 2: **(a, b, c, d)** The evolution of the control variables (solid-blue lines) and their desired targets (dashed-red lines) are shown. **(e, f)** The powers and fueling rates that are generated from the actuators (i.e., the actuator efforts u) are also shown.

$\eta_{nbi_1}, \eta_{nbi_2}, \eta_{gas}, \gamma_{pel}, \gamma_{gas}, \rho_{nbi}, \rho_{pel_1}$, and ρ_{pel_2} were set to 0.9,0.92,1,0.95,0.1,0.9,0.57,1,0.95, and 0.93, respectively. A low η_{gas} is used because gas fueling is expected be inefficient in ITER [5]. The actuators' uncertain time contains were set to be five times the expected plasma response times that are reported in [2]: $\tau_{ic}^{lag} = 1\,\text{s}$, $\tau_{ec}^{lag} = 0.1\,\text{s}$, $\tau_{pel}^{lag} = 0.5\,\text{s}$, and $\tau_{gas}^{lag} = 5\,\text{s}$. Similarly, ρ_{th}=5. The initial estimate of the composite uncertainty vector $\hat{\Theta} \triangleq (\hat{\theta}_h^T, \hat{\theta}_u^T, \hat{\theta}_e^T)^T$ was calculated by multiplying the correct values of each element, in order, with the following numbers: 1.04, 1.09, 0.92, 0.96, 1.07, 0.94, 1.03, 0.94, 1.12, 0.93, 1.05, 0.9, 1.1, 1.13, 0.9, 0.94, 0.93, 1.1, 0.88, 0.8, 1.05, 1.1, 1.1, 0.87, 0.91, 0.93, 0.96, and 0.96.

As shown in Fig. 2 (a, b, c, d), the burn control scheme was able to track the desired targets despite the numerous uncertain parameters. The target tracking was effective because the actuator allocation algorithm was able to manage the actuator efforts (Fig. 2 (e, f)) such that the burn control algorithm's control requests were satisfied. Furthermore, the burn control scheme was successful despite the fivefold increase in the actuation lags (which were assumed to be the plasma response times reported in [2]).

XI. Conclusions and Future Work

In Section X, the burn control and actuator allocation algorithms worked in tandem to overcome the challenges imposed by the presence of uncertain parameters and actuation lags. The actuator allocation algorithm presented in prior work [14] has been significantly improved upon. Uncertain parameters that were considered to be constant in [14] now vary in time. Specifically, the NBI ion-heating fraction (6), the pellet fueling efficiencies (18), and the NBI thermalization delay (21) were modeled to evolve with the plasma state. In addition, the effector system now considers gas injection and the fueling from NBI. Future work may focus on designing more complex models for the actuators. For example, pellet injection can be modeled as a discrete process where batches of particles are injected one at a time.

References

[1] J. Wesson, *Tokamaks*, 2nd ed. Oxford: Clarendon Press, 1997.

[2] J. Snipes *et al.*, "Actuator and diagnostic requirements of the ITER plasma control system," *Fusion Eng. Des.*, vol. 87, no. 12, 2012.

[3] R. Hemsworth *et al.*, "Overview of the design of the ITER heating neutral beam injectors," *New J. Phys.*, vol. 19, 2017.

[4] S. Combs *et al.*, "Overview of recent developments in pellet injection for ITER," *Fusion Eng. Des.*, vol. 87, 2012.

[5] L. Baylor *et al.*, "Pellet fuelling and control of burning plasmas in ITER," *Nucl. Fusion*, vol. 47, no. 5, pp. 443–448, May 2007.

[6] M. Boyer and E. Schuster, "Nonlinear burn condition control in tokamaks using isotopic fuel tailoring," *Nucl. Fusion*, vol. 55, no. 8, 2015.

[7] E. Schuster *et al.*, "Burn control in fusion reactors via nonlinear stabilization techniques," *Fusion Sci. Technol.*, vol. 43, no. 1, 2002.

[8] J. Martinell and J. Vitela, "An optimal burn regime in a controlled tokamak fusion power plant," in *IEEE Transactions on Plasma Science*, vol. 44, 2016, pp. 296–305.

[9] V. Graber and E. Schuster, "Assessment of the burning-plasma operational space in ITER by using a control-oriented core-SOL-divertor model," *Fusion Eng. Des.*, vol. 171, 2021.

[10] A. Pajares *et al.*, "Integrated control of individual plasma scalars with simultaneous neoclassical tearing-mode suppression," *Nucl. Fusion*, vol. 62, no. 3, 2022.

[11] N. Vu *et al.*, "Tokamak-agnostic actuator management for multi-task integrated control with application to TCV and ITER," *Fusion Eng. Des.*, vol. 147, 2019.

[12] O. Kudláček *et al.*, "Developments on actuator management, plasma state reconstruction, and control on ASDEX Upgrade," *Fusion Eng. Des.*, vol. 171, 2021.

[13] V. Graber and E. Schuster, "Nonlinear adaptive burn control and optimal control allocation of over-actuated two-temperature plasmas," in *American Control Conference*, Denver, USA, 2020.

[14] ——, "Nonlinear burn control in ITER using adaptive allocation of actuators with uncertain dynamics," *Nucl. Fusion*, vol. 62, no. 2, 2022.

[15] H. Khalil, *Nonlinear Systems*, 3rd ed. New Jersey: Prentice Hall, 2001.

[16] T. Johansen and T. Fossen, "Control allocation — a survey," *Automatica*, vol. 49, pp. 1087–1103, 2013.

[17] O. Harkegard and S. Glad, "Resolving actuator redundancy—optimal control vs. control allocation," *Automatica*, vol.49, pp.1087–1103, 2013.

[18] J. Tjonnas and T. Johansen, "Optimizing adaptive control allocation with actuator dynamics," in *2007 46th IEEE Conference on Decision and Control*, 2007, pp. 3780–3785.

[19] J. Ehrenberg, "Wall effects on particle recycling in tokamaks," in *Physical processes of the interaction of fusion plasmas with solids*. Academic Press, 1996, p. 35.

[20] H. Bosch and G. Hale, "Improved formulas for fusion cross-sections and thermal reactivities," *Nucl. Fusion*, vol. 32, no. 4, 1992.

[21] R. Gross, *Fusion Energy*. New York: Wiley-Interscience, 1984.

[22] D. Gallart *et al.*, "Modelling of ICRF heating in DEMO with special emphasis on bulk ion heating," in *AIP Conf Proc*, vol. 1689, 2015.

[23] E. Doyle *et al.*, "Chapter 2: Plasma confinement and transport," *Nucl. Fusion*, vol. 47, 2007.

[24] M. Shimada *et al.*, "Chapter 1: Overview and summary," *Nucl. Fusion*, vol. 47, 2007.

[25] Krstić *et al.*, *Nonlinear and Adaptive Control Design*. Wiley, 1995.

[26] A. Pajares and E. Schuster, "Robust nonlinear burn control in ITER to handle uncertainties in the fuel-line concentrations," *Nucl. Fusion*, vol. 59, no. 9, 2019.

[27] T. Ravensbergen *et al.*, "Density control in ITER: an iterative learning control and robust control approach," *Nucl. Fusion*, vol.58, no.1,2017.

[28] W. Li *et al.*, "A description of the ITER's gas injection systems and current R&D activities," *Fusion Eng. Des.*, vol.87, no.5, pp.813–21, 2012.